Journal of Magnetism and Magnetic Materials 324 (2012) 2315–2323

Contents lists available at SciVerse ScienceDirect

Journal of Magnetism and Magnetic Materials

journal homepage: www.elsevier.com/locate/jmmm

Fractal spectra in generalized Fibonacci one-dimensional magnonic quasicrystals

C.H.O. Costa [a], M.S. Vasconcelos [b,*], P.H.R. Barbosa [c], F.F. Barbosa Filho [c]

[a] Departamento de Física Teórica e Experimental, Universidade Federal do Rio grande do Norte, 59072-970 Natal-RN, Brazil
[b] Escola de Ciências e Tecnologia, Universidade Federal do Rio grande do Norte, 59072-970 Natal-RN, Brazil
[c] Departamento de Física, Universidade Federal do Piauí, 64049-550 Teresina-Pi, Brazil

ARTICLE INFO

Article history:
Received 13 December 2011
Received in revised form
7 February 2012
Available online 7 March 2012

Keywords:
Spin wave
Magnonic crystal
Quasiperiodic structure
Fractal spectrum

ABSTRACT

In this work we carry out a theoretical analysis of the spectra of magnons in quasiperiodic magnonic crystals arranged in accordance with generalized Fibonacci sequences in the exchange regime, by using a model based on a transfer-matrix method together random-phase approximation (RPA). The generalized Fibonacci sequences are characterized by an irrational parameter $\sigma(p,q)$, which rules the physical properties of the system. We discussed the magnonic fractal spectra for first three generalizations, i.e., silver, bronze and nickel mean. By varying the generation number, we have found that the fragmentation process of allowed bands makes possible the emergence of new allowed magnonic bulk bands in spectra regions that were magnonic band gaps before, such as which occurs in doped semiconductor devices. This interesting property arises in one-dimensional magnonic quasicrystals fabricated in accordance to quasiperiodic sequences, without the need to introduce some deferent atomic layer or defect in the system. We also make a qualitative and quantitative investigations on these magnonic spectra by analyzing the distribution and magnitude of allowed bulk bands in function of the generalized Fibonacci number F_n and as well as how they scale as a function of the number of generations of the sequences, respectively.

1. Introduction

In recent years, since the pioneering works of Yablonovitch [1] and John [2], considerable efforts have been also made in dielectric microstructures with modulated periodicity that exhibit unique properties as photonic band gaps (PBGs), i.e., the well-known photonic crystals (PCs). The concept of PBGs is quite similar to the one corresponding to electrons in solid state physics: the photon propagation is forbidden in band gap regions. Moreover, it is possible to create similar crystals for which, instead of electromagnetic waves, spin waves (SWs) are used as carriers of information. Drawing an analogy from photonic and phononic crystals (PhCs), such magnetic materials are called *magnonic crystals* (MCs) (because magnons are the quasiparticles associated to SWs).

On the other hand, magnetic structure has been few studied in the context of MCs. For example, magnetic periodic layered structures have been studied for more than two decades, where we cite, as one of the most important properties of multilayered systems, the discovery of the giant magneto-resistance effect in three-layer system containing magnetic and non-magnetic layers by Baibich et al. [3]. But, only recently Kruglyak et al. [4] proposed an experiment to investigate the physical properties of magnonic structures. They have observed that, similar to PCs, the spectrum of magnonic crystals is strongly affected by the presence of *magnonic band gaps* (MBGs), in which magnon propagation is forbidden (for review, see Ref. [5]). These results have been probed recently by Sokolovskyy et al. [6]. On the other hand, a natural extension of the concept of PCs to MCs is to consider a periodic magnetic permeability function instead of a periodic electric permissivity [7], i.e., one looks for the periodicity of the index of refraction $\eta=\sqrt{\mu}$, with $\epsilon=1$, in MCs, instead of $\eta=\sqrt{\epsilon}$, with $\mu=1$, such as occurs in PCs. This definition is compatible for spin waves in the magnetostatic regime [8]. However, for magnons in the exchange regime it is necessary to take into account that the exchange terms of magnetic materials display the same role obeyed by the permissivity function in PCs [9]. This paper is addressed to understand the thickness and localization of these MBGs, and, consequently, make us able to control the magnon propagation in such structures. For example, MCs can be used to process and transport information, being that magnon is the quasiparticle responsible for do this, exactly as occur in electronic and photonic devices.

* Corresponding author. Tel./fax: +55 84 3342 2301.
E-mail addresses: manoelvasconcelos@yahoo.com.br, mvasconcelos@ect.ufrn.br (M.S. Vasconcelos).

0304-8853 © 2012 Elsevier B.V. Open access under the Elsevier OA license.
doi:10.1016/j.jmmm.2012.02.123

Moreover, no periodic but deterministic (quasiperiodic) structures constitute a separate field of research [10,11]. There are various groups of those, namely, substitutional sequences (Fibonacci, Thue–Morse, Rudin–Shapiro, and double-period) [12,13] or fractal structures (Cantor sets or Koch fractals) [14,15]. Quasiperiodic systems do not have translational symmetry and were mainly considered as suitable theoretical models to describe the conceptual transition from a perfect periodic structure to some random version [16,17]. Specifically, MBGs were studied in *quasiperiodic magnonic crystals* or *magnonic quasicrystals* (MQCs) without [18] and with uniaxial anisotropy [19]. MQCs are defined like MCs. The difference is in the spatial distribution of the exchange terms where they are organized in quasiperiodic fashion, obeying a mathematical rule, which, here, are the *generalized Fibonacci sequences* (GFSs).

In this work, we make use of transfer-matrix method to investigate the spin waves propagation in MQCs. The calculations are carried out for the exchange dominated regime within the framework of the Heisenberg model and taking into account the random-phase approximation (RPA). The purpose of this work is to generalize previous results concerning MBGs, investigating now the generalized Fibonacci structures considering *silver* (SM), *bronze* (BM) and *nickel mean* (NM) characteristic irrational parameter, and compare them with the results for the *golden mean* (GM) case [18], which corresponds to ordinary Fibonacci sequence. The main motivation to study these structures is that they are realizable experimentally, so they are not mere academic examples of a quasicrystal. Furthermore, the trace maps of the golden, silver and bronze mean recursion relations are claimed to belong to the same universality class of dynamical systems because they possess a *invariant* trace map [20]. On the other hand, the nickel mean arrangement has a different invariant embedded within a two-dimensional plane and, thus, this sequence belongs to other universality class [21,22]. NM sequence is said to have a *pseudo-invariant* trace map. From these results, we expect to obtain some differences in magnonic spectra of silver and bronze mean in relation to nickel mean one. The theoretical investigations of physically measurable quantities, like MBGs, displaying these characteristics would be useful to check these predictions, and, surely, they can be tested experimentally.

Let us briefly review the GFSs considered in this work. These quasiperiodic structures can be obtained by an inflation rule or recursive relation, forming a binary string that can be grown by juxtaposing two building blocks A and B. Therefore, the n-th stage S_n of quasiperiodic magnonic multilayers is generated by $S_n = S_{n-1}^p S_{n-2}^q$, with $S_0 = B$ and $S_1 = A$. The indexes p and q are arbitrary positive integer numbers and $n \geq 2$. $S_n^{p(q)}$ represents $p(q)$ adjacent repetitions of the stack S_n. This type of inheritance is normal in iterative processes and frequently produces self-similar structures, which is the first indication of a fractal distribution of energy spectrum. Equivalently, they can also be generated by the recurrence relation $B \to A$, $A \to A^p B^q$, where $A^p(B^q)$ represents a string of p A's(q B's). When $p = q = 1$ we recover the well-known Fibonacci sequence. The total number of blocks A and B in S_n is equal to the *generalized Fibonacci number*, denoted by F_n, and it is given by the recurrence relation

$$F_n = pF_{n-1} + qF_{n-2}, \tag{1}$$

with initial values $F_0 = F_1 = 1$. The *characteristic irrational value* $\sigma(p,q)$, namely, the ratio F_n to F_{n-1} in the limit of $n \to \infty$, is given by the positive solution of the quadratic equation

$$\sigma^2 - p\sigma - q = 0,$$

or explicitly by

$$\sigma(p,q) = \lim_{n\to\infty} \frac{F_n}{F_{n-1}} = \frac{p + \sqrt{p^2+4q}}{2}.$$

The labels of the different types of quasiperiodic structures depend on the values of p and q. For instance, for the case $p = q = 1$, we have $\sigma(1,1) = \sigma_g = (1+\sqrt{5})/2$, the well-known *gold* or *golden mean* (*GM*) *number*. Similarly, $\sigma(2,1) = \sigma_s = 1+\sqrt{2}$ is the *silver mean* (*SM*) *number*; $\sigma(3,1) = \sigma_b = (3+\sqrt{13})/2$ is the *bronze mean* (*BM*) *number*, whereas $\sigma(1,3) = \sigma_n = (1+\sqrt{13})/2$ is the *nickel mean* (*NM*) *number*. These values of σ are the most commonly known and they are called "metallic means" [21]. Observe that σ is completely equivalent to the determination of the eigenvalues of the substitution matrix R_ρ considered by Grimm and Baake [23]. Therefore, we can classify the substitutional sequences considered in this paper based on the irrationality of $\sigma^-(p,q)$ (where the minus signal means the negative root of $\sigma(p,q)$ defined above), i.e., if $|\sigma^-(p,q)| < 1$, it is a Pisot–Vijayraghavan (PV) irrational number, and the fluctuation of the physical properties of substitution sequence is more accentuated. On the other hand, if $|\sigma^-(p,q)| > 1$, it is not a PV-type number, and, consequently, the fluctuation of its physical properties is minor. In our case, only the NM sequence is not PV-type and therefore we expect a more pronounced fluctuation of its physical properties. In actual, the SM and BM sequences are quasiperiodic, while NM case is just an aperiodic sequence [21]! In this paper we shall consider the generalized Fibonacci quasicrystals defined by $p \geq 1$, $q \geq 1$.

This paper is organized as follows. In Section 2 we present the method of calculation employed here, which is based on the transfer-matrix approach. The SW dispersion relation is then determined, and its expression follows the pattern already shown in previous works (for a review see [13]). In Section 3 we use our model to calculate the SW spectra for any generalized Fibonacci quasicrystals defined by $p \geq 1$, $q \geq 1$ (namely, silver, bronze and nickel mean). The numerical results are given in Section 4, while the some conclusions are presented in Section 5.

2. General theory

As indicated in Fig. 1a, we consider, initially, MCs in which n_A layers of material A alternate with n_B layers of material B. Initially, we analyze the periodic case, i.e., the slabs A and B alternate periodically, so that the unit cell is $[A|B]$. Later, in Section 3, we extend the results obtained here to quasiperiodic case. Both materials are taken to be simple cubic spin-S Heisenberg ferromagnetic materials, having bulk exchange constants J_A, in A, and J_B, in B, and lattice constant a for both materials, conform is schematized in Fig. 1b. The exchange terms at the interfaces are I (in $A|B$ interface), I_A (in $A|A$ interface) and I_B (in $B|B$ interface).

The Heisenberg hamiltonian for each component is (we choose units in which $\hbar = 1$)

$$H = (-1/2)\sum_{\substack{ij \\ i\neq j}} J_\alpha \vec{S}_i \cdot \vec{S}_j - g\mu_B H_0 \sum_i S_i^z, \tag{2}$$

where the sum in the first term is over sites i and nearest neighbors j, H_0 is a static external magnetic field pointing in the z-direction, and α is equal to $A(B)$, in the bulk of material $A(B)$, or $I(I_A$ or $I_B)$, in the interface $A|B$ ($A|A$ or $B|B$, respectively). The unit cell size is $D = na$, with $n = \sum_i n_{Ai} + \sum_j n_{Bj}$ (number of A-layers and B-layers in each unit cell). The l-th unit cell is defined to run from $(l-1)na + a$ to $\ln a$. At non-zero temperature the equilibrium configuration must exhibit the analogue of surface reconstruction. This implies that the mean spin S in both materials is a function of its distance from the nearest interface (in the $A|B$ interface, for

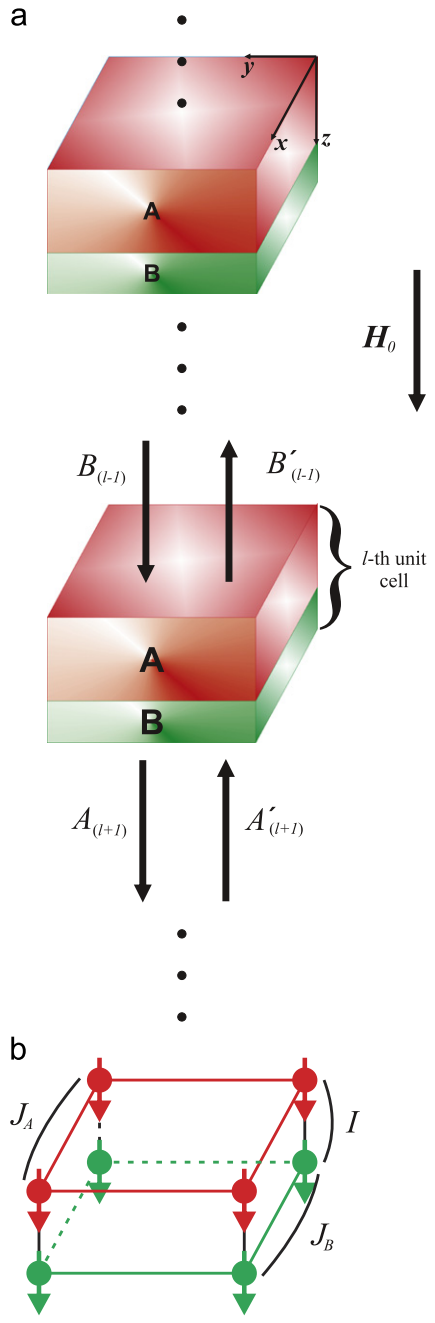

Fig. 1. Schematic representation of the MC studied here. In (a) we have the slabs A and B alternating periodically in z-direction as well as the external static magnetic field applied in the structure. The internal structure of interface $A|B$ is presented in (b), showing the spin configuration and the exchange terms in bulk and interface.

example). Although this effect is of interest, it is not our concern here, and we circumvent it by restricting our attention to the low temperature regime, $T \ll T_C$ (where T_C is Curie's temperature), at which the spins are fully ordered, i.e., we can make $\langle S^z \rangle = S$ [24].

The dispersion equation for bulk SWs in ferromagnetic medium (A or B) is found within the random-phase approximation (RPA) from the equation of motion for the spin operator $S_i^+ = S_i^x + iS_i^y$

$$i\frac{\partial}{\partial t}S_i^+ = g\mu_B H_0 S_i^+ + \langle S^z \rangle \sum_{n.n.} J_\alpha (S_i^+ - S_j^+), \tag{3}$$

where i is a given site in the bulk of ferromagnetic material. For bulk modes, S_i^+ is proportional to $e^{[i(\vec{k}\cdot\vec{r}-\omega t)]}$. Substituting this solution in Eq. (3), the dispersion relation of SWs in bulk of a ferromagnet is determined (for more details, see Refs. [13,24]), and it has the form

$$\omega = g\mu_B H_0 + J_\alpha S_\alpha [6 - \gamma(\vec{k})], \tag{4}$$

with $\gamma(\vec{k}) = 2[\cos(k_x a) + \cos(k_y a) + \cos(k_z a)]$.

The SW dispersion relation in a periodic superlattice can be found by solving the RPA equations of motion for the operators S_i^+ and using appropriate boundary conditions at the interfaces. If a given spin is not at some interface, it has the same nearest-neighbor environment, and so, has the same equation of motion as a spin in corresponding bulk medium, i.e., its relation dispersion is given by Eq. (4). On the other hand, when the spin i is located in some interface, we propose that SW amplitudes are given, within each material, by a linear combination of the positive- and negative-going solutions for the bulk medium (see Fig. 1a, for more details), i.e.,

$$S_i^+ = \{A_l e^{[i\vec{k}_A\cdot(\vec{r}-\vec{r}_{lA})]} + A'_l e^{[-i\vec{k}_A\cdot(\vec{r}-\vec{r}_{lA})]}\} e^{(-i\omega t)} \tag{5}$$

for a spin that belongs to interface from the medium A. For a spin situated at the interface of the material B, one must change the amplitudes and indexes from A to B. Here $\vec{r}_{lA}$ and $\vec{r}_{lB}$ are the positions of the left-hand layers of the corresponding component in cell l, i.e., $\vec{r}_{lA} = [(l-1)na + a]\hat{z}$ and $\vec{r}_{lB} = [(l-1)na + (n_1+1)a]\hat{z}$, and we use them in other to the transfer-matrices have the same form.

To the magnonic crystal shown in Fig. 1a, Eq. (3) at interface $A|B$ relates the amplitudes (B_l, B'_l) with (A_l, A'_l), while the same equation when applied at interface $B|A$ relates the amplitudes (A_{l+1}, A'_{l+1}) with (B_l, B'_l), and these equations can be written as follows:

$$M_A \begin{pmatrix} A_l \\ A'_l \end{pmatrix} = N_B \begin{pmatrix} B_l \\ B'_l \end{pmatrix} \tag{6}$$

and

$$M_B \begin{pmatrix} B_l \\ B'_l \end{pmatrix} = N_A \begin{pmatrix} A_{l+1} \\ A'_{l+1} \end{pmatrix}. \tag{7}$$

By means in a simple algebraic manipulation, we can associate the amplitudes (A_l, A'_l) to (A_{l+1}, A'_{l+1}), which give

$$\begin{pmatrix} A_{l+1} \\ A'_{l+1} \end{pmatrix} = N_A^{-1} M_B N_B^{-1} M_A \begin{pmatrix} A_l \\ A'_l \end{pmatrix}. \tag{8}$$

Now, using Bloch's theorem, we have that

$$\begin{pmatrix} A_{l+1} \\ A'_{l+1} \end{pmatrix} = e^{i\vec{Q}\cdot\vec{D}} \begin{pmatrix} A_l \\ A'_l \end{pmatrix}, \tag{9}$$

where $\vec{Q} = Q\hat{z}$ is Bloch's wave-vector and $\vec{D} = D\hat{z}$. In addition, we can relate the SW amplitudes in l-th unit cell with the $(l-1)$-th one. Applying Bloch's theorem for this case, we obtain the following expression:

$$\begin{pmatrix} A_{l-1} \\ A'_{l-1} \end{pmatrix} = e^{-i\vec{Q}\cdot\vec{D}} \begin{pmatrix} A_l \\ A'_l \end{pmatrix}. \tag{10}$$

From Eqs. (9) and (10), one can show that

$$\cos(QD) = (1/2)Tr[T], \tag{11}$$

with $T = N_A^{-1} M_B N_B^{-1} M_A$. The form of the matrices M's and N's can be found in Ref. [13]. Of course, T is a transfer-matrix since it relates the coefficients of the $(l+1)$-th unity cell to the coefficients of the l-th unity cell. The last line follows from the fact that T is an unimodular 2×2 matrix. Eq. (11) describes the SWs bulk modes in a periodic arrangement of the magnetic multilayers.

Although, in this work, we are concerned in study the distribution of magnonic bulk bands, for completeness we remark that a similar expression can be obtained for surface SWs. These surface magnons are modes that decay exponentially from interface, but they have an oscillatory behavior in-plane component of wave-vector, and this allows that the mode propagate only in surface. By considering the truncation of the MC, considered in Fig. 1, at the plane $z=0$, we can replace Q by iβ in Eq. (11) (with $\mathrm{Re}(\beta)>0$), in such way that Bloch's theorem holds provided [13,18]). Besides of this, in MCs, we also can find the so-called interfacial SWs, which are modes that can propagate between the interfaces, since that some conditions be obeyed, like the SWS wave-vector direction in plane of multilayer. For a review about interfacial magnons, see Refs. [25–27].

Once we know the form of the transfer-matrix T, the bulk SW spectra are determined. If we have an $A|A(B|B)$ interface, we only need to change the interface exchange constant from I to $I_A(I_B)$. This not modifies the functional form of the matrices. This expression also holds for any other arrangement of the magnetic multilayers, and therefore will be employed in the determination of the spectra for the quasiperiodic structures.

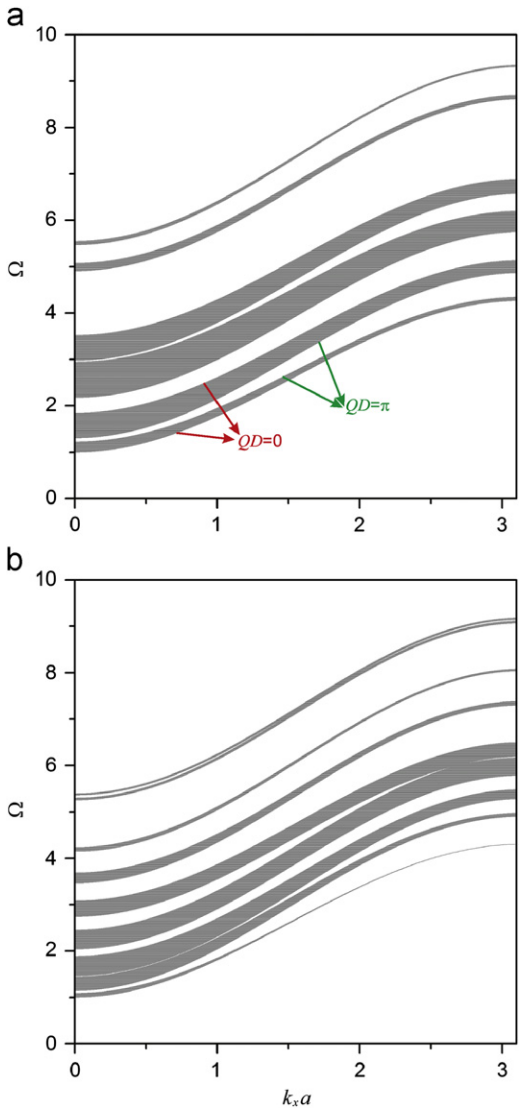

Fig. 2. Magnon spectrum as function of the reduced frequency Ω versus the dimensionless wave-vector $k_x a$: (a) in a MC (which correspond to second generation of Fibonacci GM sequence, i.e., $n=2$) and which unit cell is $[A|B]$; and (b) in a MQC (third generation of Fibonacci GM, i.e., $n=3$), with unit cell being $[A|B|A]$. The shadow areas represent the magnonic bulk bands and they are limited by $QD=0$ and $QD=\pi$. Between these bulk bands there are gap regions, that are the magnonic band gaps. In these regions, the magnonic surface modes can propagate in the surface of the structure.

3. Transfer-matrix approach for the quasiperiodic structures

We now intend to investigate the bulk SWs in generalized Fibonacci one-dimensional MQCs by using the calculations of the previous section. A generalized Fibonacci structure, as discussed previously, can be grown by juxtaposing two building blocks A and B (corresponding to layers A and B), in such a way that the n-th stage of the sequence S_n is given iteratively by the rule $S_n=S_{n-1}^p S_{n-2}^q$, for $n\geq 2$, with $S_0=B$ and $S_1=A$. It is also invariant under the transformations $A\to A^pB^q$ and $B\to A$. We recall the transfer-matrix for any generation of an *Fibonacci golden mean* MQC is [18]

$$T_{S_n}=T_{S_{n-2}}T_{S_{n-1}},\quad n\geq 3, \tag{12}$$

where $T_{S_1}=N_{AA}^{-1}M_{AA}$ and $T_{S_2}=N_A^{-1}M_BN_B^{-1}M_A$.

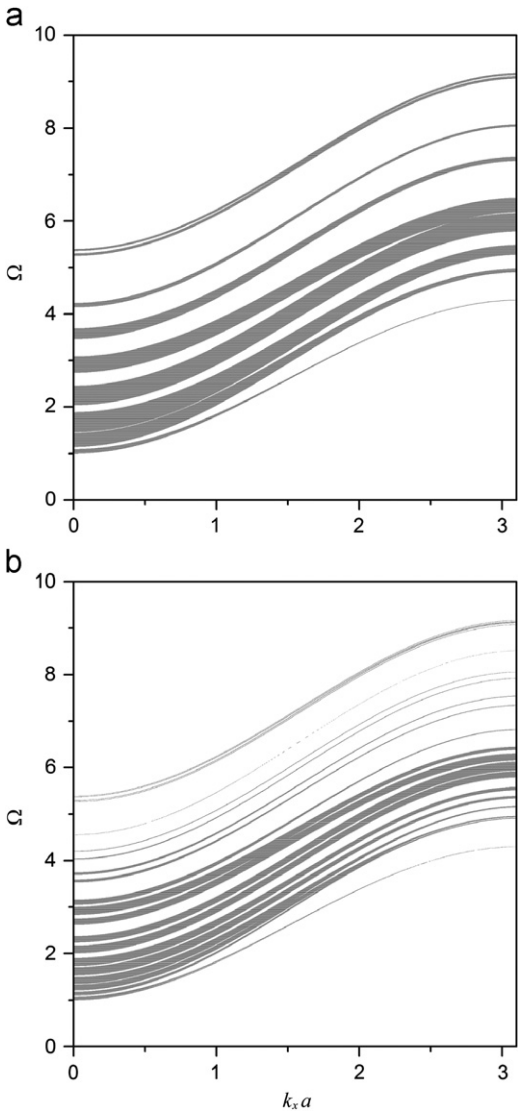

Fig. 3. Same as Fig. 2, but for (a) second ($n=2$) and (b) third ($n=3$) generations of Fibonacci silver mean MQC. The number of allowed and gap bands raise because of growing of unit cell. On the other hand, the allowed band widths are narrower.

However, to *Fibonacci silver mean* structures, the transfer-matrix for any generation can be obtained by following equation:

$$T_{S_n} = T_{S_{n-2}} T_{S_{n-1}} T_{S_{n-1}} = T_{S_{n-2}} (T_{S_{n-1}})^2, \quad n \geq 3, \tag{13}$$

where, now, $T_{S_2} = N_A^{-1} M_B N_B^{-1} M_A N_{AA}^{-1} M_{AA}$. Similarly, to *Fibonacci bronze mean* MQCs, the transfer-matrix obeys the following recurrence relation:

$$T_{S_n} = T_{S_{n-2}} T_{S_{n-1}} T_{S_{n-1}} T_{S_{n-1}} = T_{S_{n-2}} (T_{S_{n-1}})^3, \quad n \geq 3, \tag{14}$$

with $T_{S_2} = N_A^{-1} M_B N_B^{-1} M_A N_{AA}^{-1} M_{AA} N_{AA}^{-1} M_{AA}$.

For completeness, we want to investigate also the *Fibonacci nickel mean* MQCs. The transfer-matrix for the n-th generation is given by

$$T_{S_n} = T_{S_{n-2}} T_{S_{n-2}} T_{S_{n-2}} T_{S_{n-1}} = (T_{S_{n-2}})^3 T_{S_{n-1}}, \quad n \geq 3, \tag{15}$$

and $T_{S_2} = N_A^{-1} M_B N_{BB}^{-1} M_{BB} N_{BB}^{-1} M_{BB} N_B^{-1} M_A$.

We can extend the transfer-matrix method for a generalized Fibonacci sequence for any values of p and $q \geq 1$. It is easy to show that the transfer-matrix for the n-th generation of the sequence $\sigma(p,q)$ is given by

$$T_{S_n} = (T_{S_{n-2}})^q (T_{S_{n-1}})^p, \quad n \geq 3, \tag{16}$$

where $(T_{S_n})^{p(q)}$ means that matrix T_{S_n} is multiplied $p(q)$ times. Therefore, from the knowledge of the transfer matrices T_{S_1} and T_{S_2} we can determine the transfer-matrix of any generation, and they are given by $T_{S_1} = N_{AA}^{-1} M_{AA}$ and $T_{S_2} = N_A^{-1} M_B (N_{BB}^{-1} M_{BB})^{(q-1)} N_B^{-1} M_A (N_{AA}^{-1} M_{AA})^{(p-1)}$.

With the knowledge of all those transfer matrices, together with Eq. (11), we can now calculate the SW spectra (bulk modes) for these artificial structures and this is the topic of the next section.

4. Numerical results

In this section we present some numerical illustrations of magnonic band structures for MQCs, as a function of the reduced frequency $\Omega = \omega / J_A S_A$ versus the dimensionless wave-vector $k_x a$, k_x being the in-plane wave-vector (throughout our study, we choose $k_y a = 0$), a is the lattice constant, and versus n, the generation number of GFSs. In addition, we show the power law plots for SM, BM, and NM sequences. In what follows, the physical parameters used are the number of layers in each material

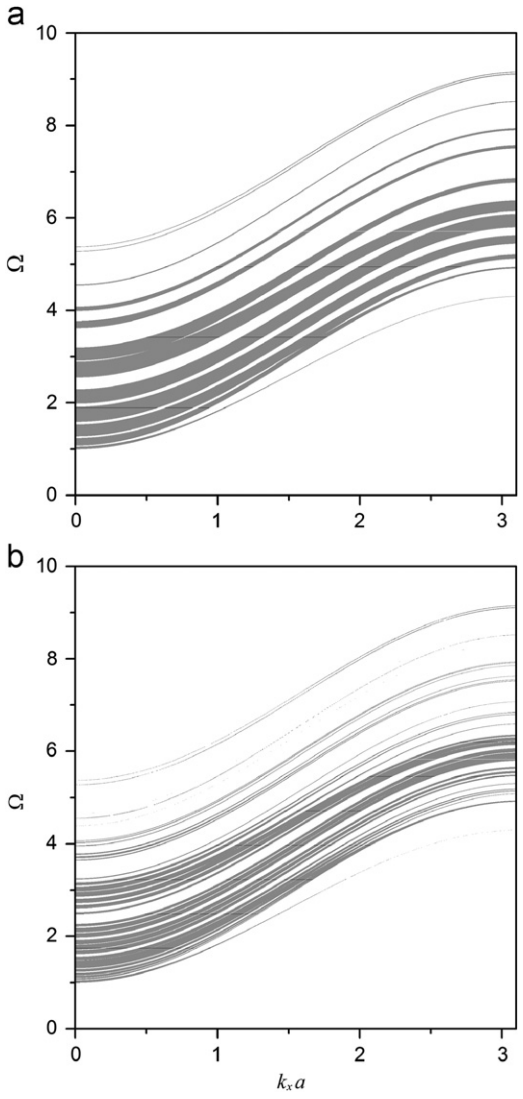

Fig. 4. Similar to Fig. 2, we plot the Fibonacci BM case for second (a) and third (b) generations of MQC.

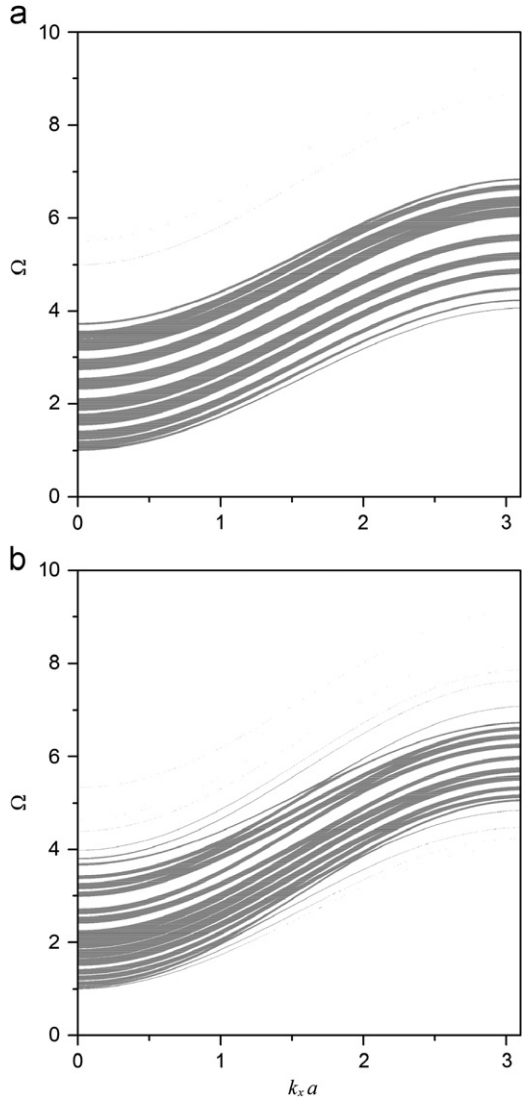

Fig. 5. The Fibonacci NM case is shown for your second (a) and third (b) generations of MQC, in similar way to Fig. 2. In this case, we can note the more pronounced fluctuation on the magnon spectrum, as we expected for NM sequence ($|\sigma^-(1,3)|$ is not PV-type).

$n_A = n_B = 3$, respectively; the average spins $S_A = 1.0$ and $S_B = 1.5$, respectively; the ratio between the exchange terms $J_{AB} = J_A/J_B = 2.0$, $I_{AA} = I_A/J_A = I_{BB} = I_B/J_B = 0.8$, $I_A = I/J_A = 1.2$, $I_B = I/J_B = 2.4$, $H_{0A} = g\mu_B H_0/J_A = 1.0$ and $H_{0B} = g\mu_B H_0/J_B = 2.0$.

In Figs. 2–5, the bulk bands for magnons in MQCs are represented by shaded areas, and they are limited by $QD = 0$ and $QD = \pi$ (see Fig. 2a). Between these bulk bands there are gap regions, which are the magnonic band gaps. However, we can have also the propagation of surface modes or surface SWs in these gap regions [18].

In Fig. 2a, we present the well-known *periodic case*, whose structure is shown in Fig. 1, and which corresponds to *second generation* ($n = 2$) of Fibonacci GM sequence. This band structure is the "basic signature" of a MC, showing various band gaps (the white regions between the shaded ones), and so, characterizing a band pass structures, as is found in electronic and photonic crystals. This is the operating mechanism of multiplex devices, in which many narrow bulk bands exist in a short frequency range. Such devices make possible the data transmission in very well-defined frequencies. The SW spectrum for *third generation* ($n = 3$) is presented in Fig. 2b, where we can see that more bulk bands emerge and they are narrower than Fig. 2a. The number of bulk bands increases because of the growing of the layers in the unit cell. In Fig. 2a, the unit cell is $[A|B]$, with six layers total, while in Fig. 2b, the unit cell is formed by $[A|B|A]$, with nine layers total. Thus, the bulk bands are narrower and, consequently, more MBGs arise up.

In Fig. 3, we have the same as Fig. 2, but for the *second* (Fig. 3a) and *third* (Fig. 3b) *generations* of Fibonacci SM sequence, while in Fig. 4, we plot the Fibonacci BM case: *second* (Fig. 4a) and *third* (Fig. 4b) *generations*. The Fibonacci NM case is shown in Fig. 5 for your *second* (Fig. 5a) and *third* (Fig. 5b) *generations* too. Comparing the magnon spectra for the second generation of each sequence presented, we observe that the spectra display allowed bands more narrowed (see Figs. 2a, 3a, 4a and 5a). The same behavior is observed to the third generation. Here, what happens is that the sequences grow up more rapidly when values of p and q increase. In this point, we call attention to localization phenomena, which

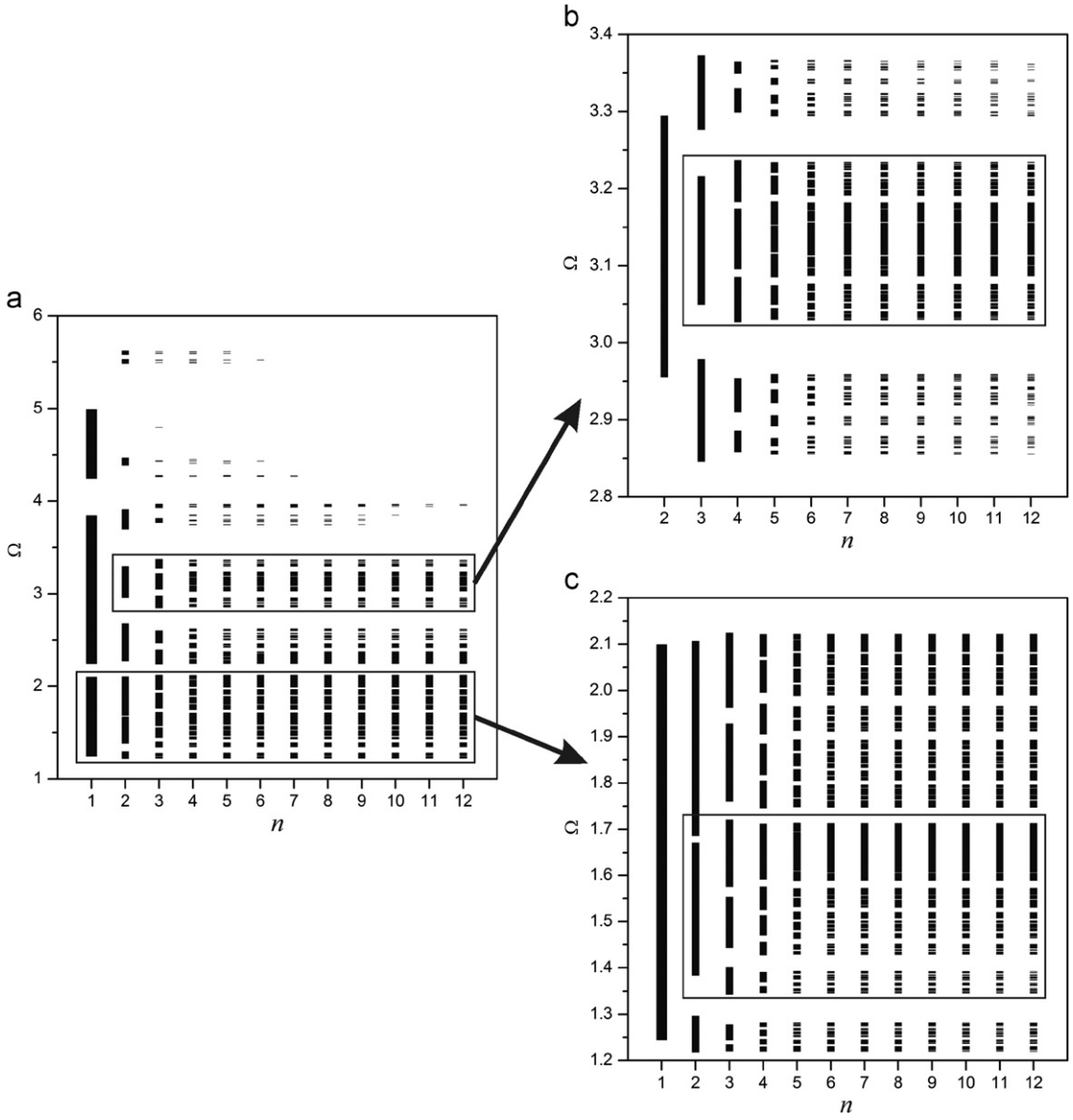

Fig. 6. Distribution of the magnonic allowed bandwidths for the Fibonacci silver mean MQC as a function of the Fibonacci SM generation number n, for $k_x a = 0.5$. Here, to characterize the self-similar behavior of spectrum, we present a zoom of the regions surrounded by a line box in (a), (b) and (c) are the amplification of the regions in (a).

is linked with the narrowing of allowed bands. This narrowing of the bulk bands is due to the growing of the unity cell, and this behavior appears in other quasiperiodic systems [13,14].

Another very important property observed in Figs. 2–5 is that, by varying the generation number n, the fragmentation process of allowed bands make possible the emergence of new allowed magnonic bulk bands in regions of the spectra that were magnonic band gaps before. This is observed more clearly in Figs. 6–8. Physical properties like that frequently occur in semiconductor crystals when we dope it with impurities or defects. This interesting property arises in one-dimensional magnonic quasicrystals fabricated in accordance to quasiperiodic sequences, without the need to introduce some deferent atomic layer or defect in the system. In other words, we can create propagation modes in band gap regions using a multilayer system formed by homogenous material arranged in accordance with some quasiperiodic sequence just modifying the number of the generations of the sequence used! This can be verified comparing the second and third generation's spectra presented.

As follows, in Fig. 6, we make a qualitative investigation about the self-similarity and fractal behavior of the magnonic spectra showed previously by plotting the forbidden and allowed energies of the bandwidths of the magnonic spectra in the Fibonacci silver mean sequence against the Fibonacci SM generation number n, up to the 12th generation of this sequence (we fixed $k_x a = 0.5$). The number of magnonic band pass is equal to three times the generalized Fibonacci number of the correspondent generation. Note that, as expected, for large n the magnonic allowed band regions get narrower and narrower, as an indication of more localized modes, as discoursed above, and they have a typical self-similar Cantor set structure. In Fig. 6b and c, in order to show the self-similar behavior of spectrum, we present a zoom of the regions surrounded by a line box in Fig. 6a. We can observe that Fig. 6b and c is similar, except by scale, stressing the self-similar feature, and, in themselves, we can identify other self-similar regions. In Figs. 7 and 8, we make the same procedure as in Fig. 6, but for Fibonacci BM and NM, respectively, showing the self-similarity only for BM case (see Fig. 7b and c). For NM case, we do not find self-similarity as in the other cases. As we have commented at Section 1, this behavior was expected once the NM sequence belongs to another universality class characterized by PV irrational number. In SM and BM cases, we found that one

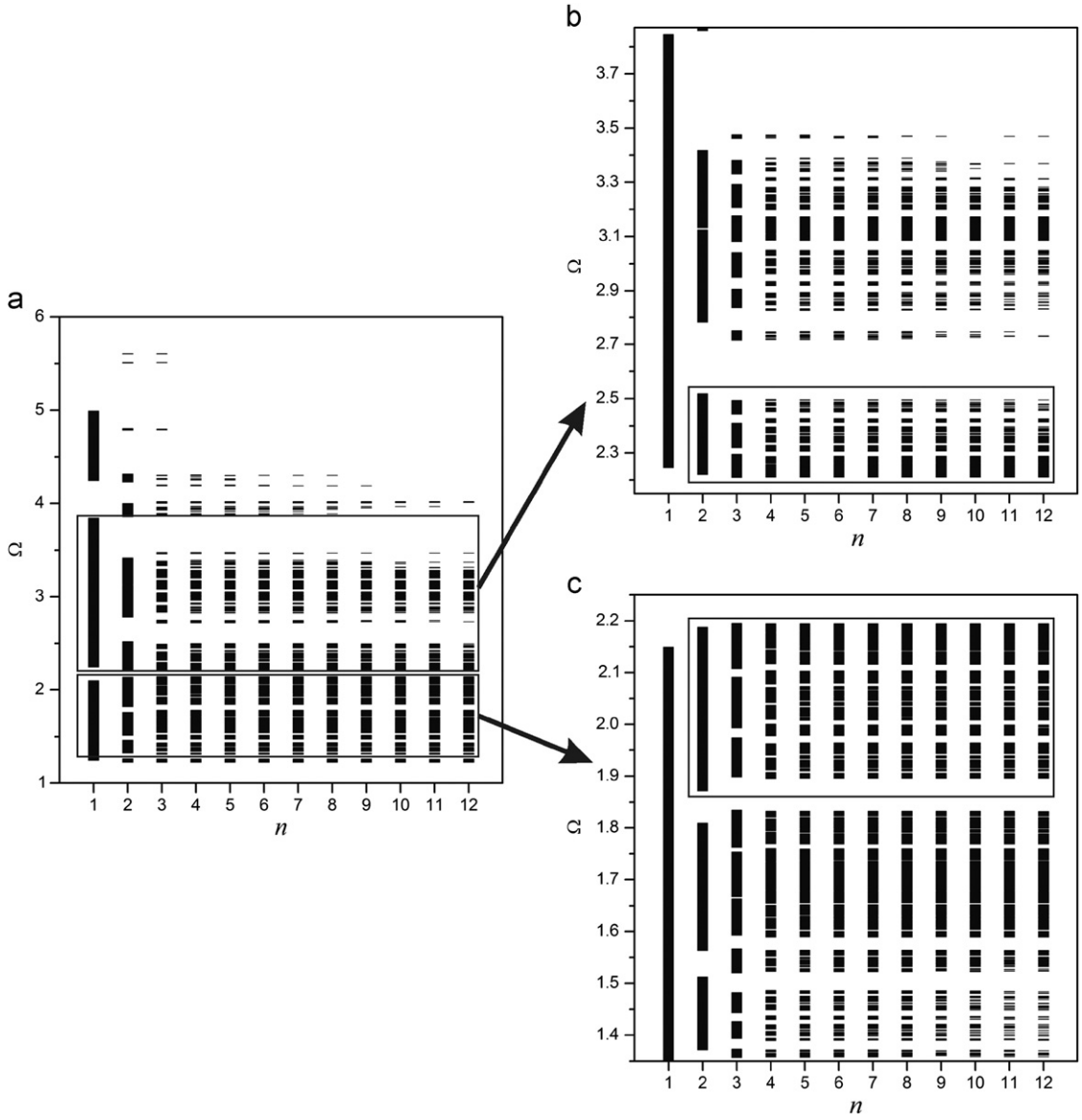

Fig. 7. Similar to Fig. 6, but for the Fibonacci BM sequence. The line box in this figure is to characterize the self-similar behavior of spectrum, in the same way presented in Fig. 6.

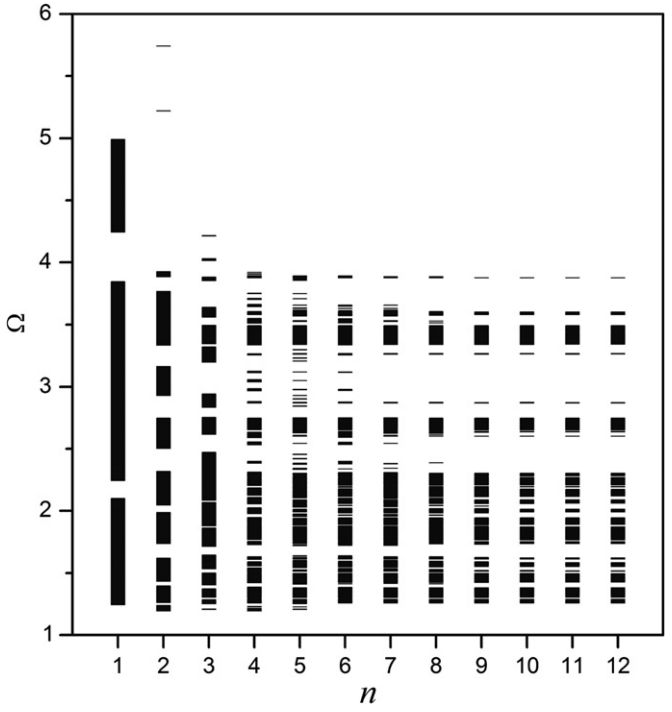

Fig. 8. Same as Fig. 6, but for the Fibonacci NM sequence. In similar way to Fig. 5 case, we can note the more pronounced fluctuation on the power law, as we expected for NM sequence ($|\sigma^{-}(1,3)|$ is not PV-type).

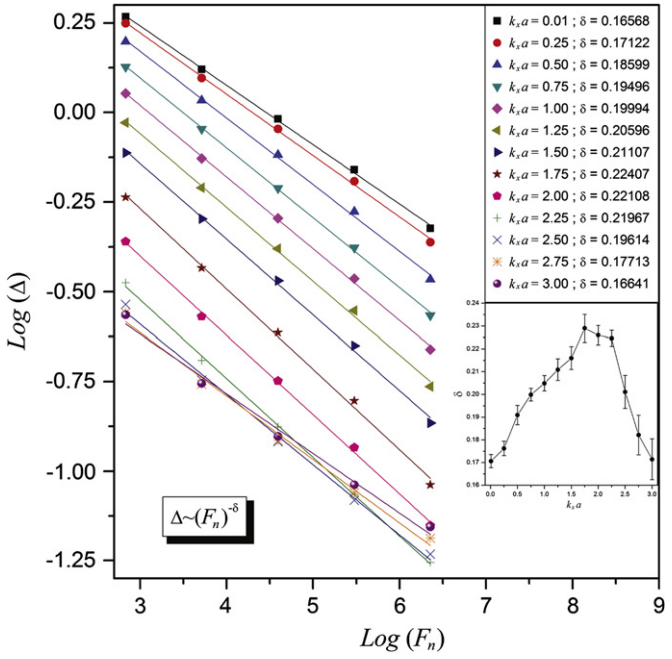

Fig. 9. The log–log plot for the full magnonic spectrum in the Fibonacci SM case. The inset shows the dependence of exponent δ in function of $k_x a$, together the error bar, that is approximately 10^{-4}. In the legend we have the $k_x a$ values used here.

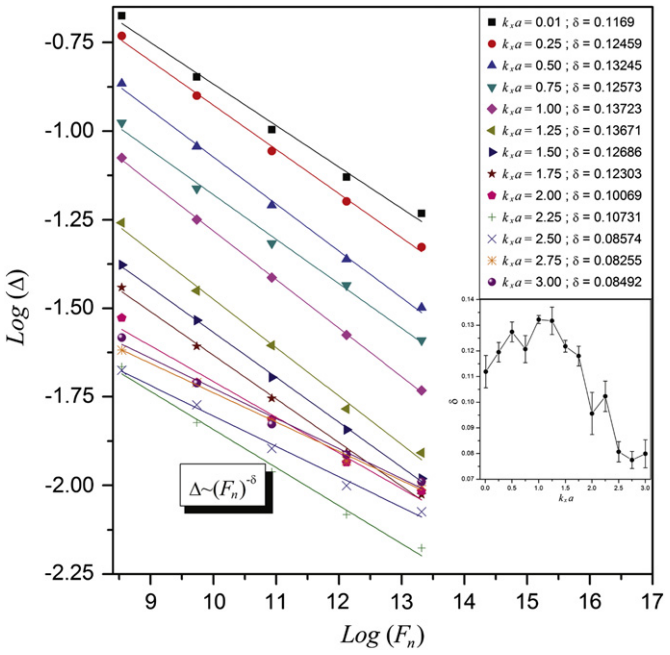

Fig. 10. Same as Fig. 9, but for the Fibonacci BM sequence.

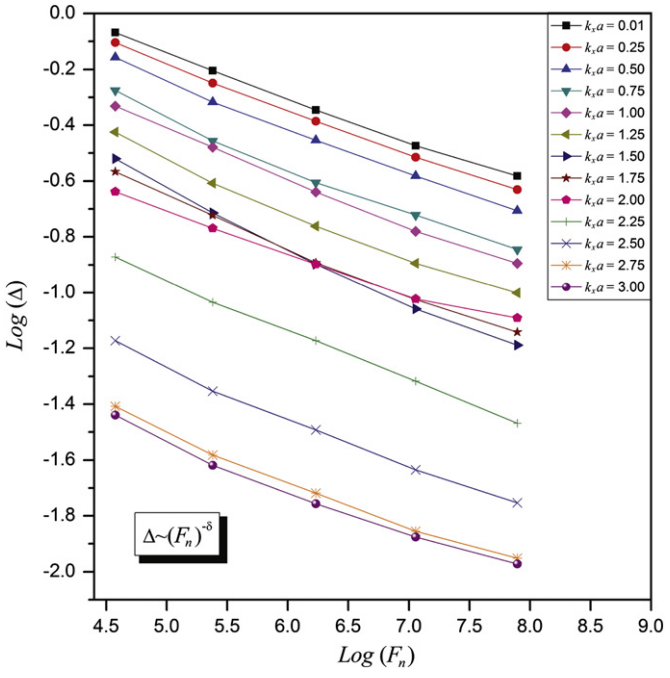

Fig. 11. Same as Fig. 9, but for the Fibonacci NM sequence. Here we can observe the pronounced fluctuation on the dependence of exponent δ in function of $k_x a$, as we expected for NM sequence.

allowed band is "broken" giving origin to three ones, characterizing a trifurcation of bulk band, exactly as occurs in PCs [28].

Now, we also make a quantitative study about the spectra of the sequences studied here. So, we investigate the power laws behavior, which are typically found in this kind of system. We find here that the narrowing phenomena of the band pass is governed by the power law $\Delta \sim F_n^{-\delta(k_x a)}$, where Δ is the total width of the allowed bands, F_n is the generalized Fibonacci number, and the exponent $\delta(k_x a)$ can be identified as being a *diffusion constant* of the spectra [14] (which, in principle, can be related to the dimensionless wave vector $k_x a$) and one can relate it with the fractal dimension of the spectrum. In Fig. 9 we show a log–log plot of these power laws for the full spectrum and for different values of $k_x a$, starting on $k_x a = 0.01$ up to $k_x a = 3.0$, for Fibonacci SM. One can see that, for the full magnonic spectrum, there is a dependence of the δ exponent with the common in-plane wave vector $k_x a$, which is not linear. The inset in Fig. 9 shows us that δ increases in the interval $0 \leq k_x a \leq 1.75$. For $k_x a \geq 1.75$, δ decreases

up to your minimum value, that is approximately equal to your initial value $\delta(k_x a = 0.01) = 0.165$. In this figure, we can observe that magnonic spectrum has a fractal behavior, confirmed by the power law! Also, we can compare this result with the case studied by Anselmo et al. [30], where they have investigated this scale exponent for magnetostatic spin waves in Fibonacci GM, Thue–Morse and double-period quasiperiodic systems. They have showed that, for the k_x values starting in the begin of Brillouin zone ($k_x a = 0$) until the center of the Brillouin zone ($k_x a = \pi/2$), the δ exponent increases monotonically, as found in the inset of Fig. 9. Therefore, this fact indicates that this feature could be independent of the system.

In Figs. 10 and 11, we have same as in Fig. 9, however, for Fibonacci BM and NM sequences. To the former, we found that the spectrum present a fractal behavior too! The inset in Fig. 10 shows us that δ increases until your maximum value, $\delta(k_x a = 1.0) = 0.137$. When $k_x a \geq 1.0$, δ decreases up to your minimum value that is, approximately, $\delta(k_x a = 2.75) = 0.082$.

5. Conclusions

In this work we presented a general theory for the propagation of magnons in one-dimensional MQCs fabricated in a quasiperiodic fashion in accordance with the generalized Fibonacci recurrence relation. We present the magnonic relation dispersion spectra for SM, BM and NM cases, and compare them with ones of the GM case. We could observe that MQCs are systems that have spectra containing a very rich band pass structure, and, therefore, it is suitable be used as multiplex logical gates systems [29].

Another interesting property found in magnonic GFSs spectra is the self-similar behavior of magnonic bulk bands in function of the generalized Fibonacci generation number n, where, in the limit $n \to 0$, these spectra become a Cantor fractal. Moreover, for a given generation, we found that one bulk band is split into three other bulk bands, at each generation, revealing a trifurcation property of spectra. This self-similar behavior is found just for SM and BM sequences, due to the reason $\sigma^-(p,q)$ to be classified as PV irrational number. As discussed before, for NM, $\sigma^-(p,q)$ is not a PV number; so, it belongs to different class universality, and this fact is evidenced in this qualitative analysis of magnonic allowed bands.

A quantitative analysis is made for Fibonacci silver and bronze mean cases, where we show that a sum of allowed band width Δ scales with the generalized Fibonacci number F_n by mean the δ exponent, giving a power law $\Delta \sim (F_n)^{\delta}$ which has a strong dependence on dimensionless wave-vector $k_x a$. The NM sequence does not obey a power law, once that its spectra are not self-similar. For the Fibonacci SM, we found that δ increases monotonically with $k_x a$, this being between 0 and $\pi/2$, in according with the result in [30]; while that, for BM, we found a non-linear dependence of δ with $k_x a$.

Recent developments in the experimental techniques applicable to magnetic systems allow the experimentalists to consider and investigate the possibility of magnons be used either to transmit or process information [31–34]. For example, standing spin waves have been observed in micron sized thin-films metallic elements by mean time-resolved scanning Keer microscopy (TRSKM) and Brillouin light scattering [31,32]. More recently, Kruglyak and Hicken have proposed an experiment that can facilitate the investigations of magnons propagation with wavelengths below of several nanometers and frequencies in excess of hundreds of Gigahertz [34]. These experiments could be used to probe the spectra studied here. We hope that this work could be inspiring the experimentalists to study further research in this area.

Acknowledgments

We would like to thank partial financial support from the Brazilian Research Agencies CNPq, Capes, Propesq-UFPI.

References

[1] E. Yablonovitch, Physical Review Letters 58 (1987) 2059.
[2] S. John, Physical Review Letters 58 (1987) 2486.
[3] M.N. Baibich, J.M. Broto, A. Fert, F.N. Vandau, F. Petroff, P. Eitenne, G. Creuzet, A. Friederich, J. Chazelas, Physical Review Letters 61 (1988) 2472.
[4] V.V. Kruglyak, R.J. Hicken, Journal of Magnetism and Magnetic Materials 306 (2006) 191.
[5] V.V. Kruglyak, S.O. Demokritov, D. Grundler, Journal of Physics D: Applied Physics 43 (2010) 264001.
[6] M. Sokolovskyy, M. Krawczyk, Journal of Nanoparticle Research, Special Issue: Nanostructured Materials 2010 (2011) 1, (http://dx.doi.org/10.1007/s11051-011-0303-5).
[7] A. Kozhanov, D. Ouellette, Z. Griffith, M. Rodwell, A.P. Jacob, D.W. Lee, S.X. Wang, S.J. Allen, Applied Physics Letters 94 (2009) 012505.
[8] D.H.A.L. Anselmo, M.G. Cottam, E.L. Albuquerque, Journal of Physics: Condensed Matter 12 (2000) 1041.
[9] D.D. Stancil, A. Prabhakar, Spin Waves: Theory and Applications, Springer, Heidelberg, 2009.
[10] P.J. Steinhardt, Endeavour 14 (1990) 112.
[11] G. Coddens, P. Launois, Endeavour 20 (1996) 16.
[12] M.S. Vasconcelos, E.L. Albuquerque, Physical Review B 57 (1998) 2826.
[13] E.L. Albuquerque, M.G. Cottam, Polaritons in Periodic and Quasiperiodic Structures, Elsevier, Amsterdam, 2004.
[14] M.S Vasconcelos, E.L. Albuquerque, Physica B 222 (1996) 113.
[15] A.V. Lavrinenko, S.V. Zhukovsky, K.S. Sandomirski, S.V. Gaponenko, Physical Review E 65 (2002) 036621.
[16] T. Okamoto, A. Fukuyama, Optics Express 13 (2005) 8122.
[17] L.A. Chernov, Wave Propagation in a Random Medium, McGraw-Hill, 1961.
[18] C.G. Bezerra, E.L. Albuquerque, Physica A 245 (1997) 379. (255 (1998) 285).
[19] C.G. Bezerra, E.L. Albuquerque, E. Nogueira Jr, Physica A 267 (1999) 124.
[20] G. Gumbs, M.K. Ali, Physical Review Letters 60 (1988) 1081.
[21] P.W. Mauriz, M.S. Vasconcelos, E.L. Albuquerque, Physica A 329 (2003) 101.
[22] M. Kolář, M.K. Ali, Physical Review B 39 (1989) 426.
[23] U. Grimm, M. Baake, Aperiodic Ising models, in: The Mathematics of Long-Range Aperiodic Order, Kluwer, Dordrecht, 1997.
[24] M.G. Cottam, D.R. Tilley, Introduction to Surface and Superlattice Excitations, second ed., Taylor & Francis, 2004.
[25] H. Puszkarski, A. Akjouj, B. Djafari-Rouhani, L. Dobrzynski, Physical Review B 51 (1995) 16008.
[26] G.H. Yun, X.X. Liang, European Physical Journal B 35 (2003) 261.
[27] W.P. Zhou, G.H. Yun, X.X. Liang, European Physical Journal B 55 (2007) 37.
[28] Z.X. Liu, L.M. Wang, H. He, W.Y. Zhang, European Physical Journal B 59 (2007) 179.
[29] A. Khitun, M. Bao, K.L. Wang, Journal of Physics D: Applied Physics 43 (2010) 264005.
[30] D.H.A.L. Anselmo, G.A. Farias, R.N. Costa, E.L. Albuquerque, Physica A 286 (2000) 283.
[31] A. Barman, V.V. Kruglyak, R.J. Hicken, A. Kundrotaite, M. Rahman, Applied Physics Letters 82 (2003) 3065.
[32] K. Perzlmaier, M. Buess, C.H. Back, V.E. Demidov, B. Hillebrands, S.O. Demokritov, Physical Review Letters 94 (2005) 57202.
[33] M.P. Kostylev, A.A. Serga, T. Schneider, B. Leven, B. Hillebrands, Applied Physics Letters 87 (2005) 153501.
[34] Y. Au, T. Davison, E. Ahmad, P.S. Keatley, R.J. Hicken, V.V. Kruglyak, Applied Physics Letters 98 (2011) 122506.